JACS
JOURNAL OF THE AMERICAN CHEMICAL SOCIETY
Article
pubs.acs.org/JACS

Sequence-specific Nucleic Acid Detection from Binary Pore Conductance Measurement

Leyla Esfandiari,[†] Harold G. Monbouquette,*[,‡] and Jacob J. Schmidt*[,†]

[†]Department of Bioengineering, University of California, Los Angeles, California, United States
[‡]Department of Chemical and Biomolecular Engineering, University of California, Los Angeles, California, United States

Supporting Information

ABSTRACT: We describe a platform for sequence-specific nucleic acid (NA) detection utilizing a micropipet tapered to a 2 μm diameter pore and 3 μm diameter polystyrene beads to which uncharged peptide nucleic acid (PNA) probe molecules have been conjugated. As the target NAs hybridize to the complementary PNA-beads, the beads acquire negative charge and become electrophoretically mobile. An applied electric field guides these NA-PNA-beads toward the pipet tip, which they obstruct, leading to an indefinite, electrically detectable, partial blockade of the pore. In the presence of noncomplementary NA, even to the level of single base mismatch, permanent pore blockade is not seen. We show application of this platform to detection of the anthrax lethal factor sequence.

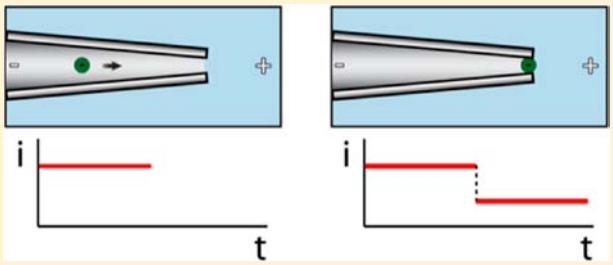

1. INTRODUCTION

Detection of specific DNA or RNA sequences is highly desired in a range of diverse applications such as screening for genetic diseases,[1−3] pathogenic microbe identification for food safety,[4−6] and paternity tests in forensic science.[7,8] For many, if not most, of these applications, the paramount need is for a yes or no answer (binary response) regarding the presence or absence of the nucleic acid (NA) sequence of interest in a sample rather than a quantitative determination of concentration. The majority of conventional sequence-specific DNA or RNA detection platforms also rely on base pairing interaction between two single strands of complementary nucleic acids that can be detected by optical, mechanical, or electrochemical readout.[9] Many of these platforms require amplification by polymerase chain reaction, fluorescent or enzymatic labels, and expensive instrumentation.[10,11]

Recently, biological or solid-state nanopores have been used as sequence specific NA detection platforms.[12−15] Nanopores are attractive for label-free molecular sensing, because the presence of single objects within the pore, down to molecular in size, can result in large modulations of pore electrical conductance. In most of this work, these conductance modulations are transient and rapid, occurring as the object passes through the pore, and therefore a fast and sensitive amplifier is required.

We have developed a binary, sequence-specific NA detection concept based on permanent attenuation of nanopore conductance by electrophoretically mobile beads. This approach provides a yes or no signal as to the presence of a target NA in a sample, but in its current embodiment, it does not give concentration data. Sequence specificity is achieved using peptide nucleic acid (PNA) probe molecules conjugated to the beads.[16] PNA has been used previously for sequence-specific DNA detection in a number of platforms,[17−27] including electrochemical detection of DNA hybridization with PNA-modified magnetic beads[28] and detection of DNA hybridization to PNA bound to the walls of a nanopore sensor.[29,30] PNA offers many advantages over DNA probes including resistance to enzyme-catalyzed degradation, increased stability of complementary DNA complexes, and increased sensitivity of these complexes to single base pair mismatches.[3,31] Here we take particular advantage of the electrical neutrality of PNA to ensure that the beads are uncharged and electrophoretically immobile until target NA is complexed. Hybridization of complementary target NA to the PNA-beads imparts sufficient negative charge to the beads, enabling them to be driven electrophoretically to the pore. The beads then physically occlude the pore, leading to a large decrease in conductance. The coupling of target NA to the PNA-bead conjugate thereby leads to an electromechanical amplification phenomenon that gives rise to a large, easily detected, binary modulation of electrical current. The "pores" used in the proof-of-concept work described here are the capillary openings formed at prepulled glass micropipet tips. Similar glass pores have been used to detect single DNA molecules attached to a 10 nm gold nanoparticle[32] and the folding state of double-stranded DNA,[33] in addition to their use for electrochemical readout of NA binding events.[34,35] The label-free, potentially low cost sensor with a simple binary read-out described here may have significant technological appeal.

Received: June 18, 2012
Published: August 29, 2012

   dx.doi.org/10.1021/ja3059205 | J. Am. Chem. Soc. 2012, 134, 15880−15886

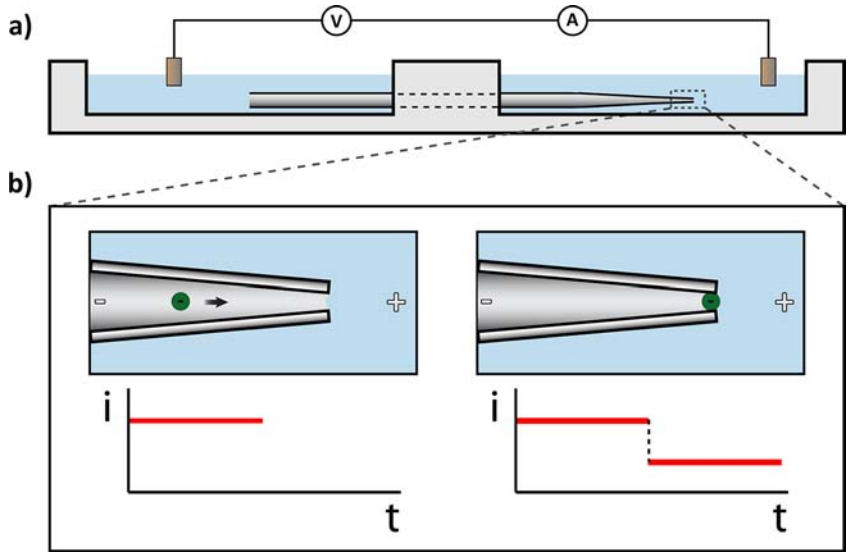

Figure 1. (a) Cross-sectional diagram of the pipet and measurement chamber. (b) Depiction of pipet tip and measured current before bead blockade (left) and after (right).

2. PROCEDURE

2.1. Materials. All chemicals were purchased from Sigma-Aldrich (St. Louis, MO) unless otherwise noted. Amine and carboxylic acid-functionalized 3 μm diameter polystyrene microspheres were purchased from Polysciences, Inc. (Warrington, PA). All oligonucleotides (PNA and single stranded DNA) were purchased from Bio-Synthesis, Inc. (Lewisville, TX) as HPLC purified and lyophilized powders. Single stranded DNA (ssDNA) molecules used were: polyT (5′-TT TT TT TT TT TT TT TT TT-3′), polyA (5′- AA AA AA AA AA AA AA AA AA-3′), anthrax LF (5′-GG AT TA TT GT TA AA AA AA AA-3′), and anthrax LF with single base mismatch (5′-GG AT TC TT GT TA AA AAAA AA-3′). The PNA capture probes used were amine-TT TT TT TT TT TT and amine-$(CH_2CH_2O)_{12}$- CC TA AT AA CA AT. Prepulled borosilicate micropipets with 2 μm pore diameter were purchased from World Precision Instruments, Inc. (Sarasota, FL).

2.2. Probe Coupling to Microspheres. Fifty microliters of 3 μm, carboxylic acid-functionalized polystyrene microspheres at 1.69×10^9/mL were washed three times with MES buffer (60 mM 2-(*N*-morpholino) ethanesulfonic acid, pH 5.5). After each wash the microspheres were centrifuged at 14 000 rpm for 15 min; at the end of the last wash they were resuspended into 0.6 mL coupling buffer (100 mM1-[3-(dimethylamine) propyl]-3-ethylcarbodiimide (EDC) in MES buffer). Ten nanomoles of amine-functionalized PNA probes were added to the coupling buffer with beads and incubated at 50 °C for 3 h. The beads were then washed once in 0.4× SSC buffer (60 mM NaCl, 6 mM trisodium citrate, 0.1% Triton X-100, pH 8), resuspended into 0.6 mL of coupling buffer containing 100 mM ethanolamine, and incubated at 50 °C for one hour to cap any remaining unreacted carboxylic groups with ethanolamine. After the last coupling step, the beads were washed 4 times in 0.4× SSC buffer and were stored in PBS buffer at 4 °C.

2.3. Hybridization Assay. Prior to DNA incubation, PNA-beads were washed twice in 0.4× SSC buffer and once in hybridization buffer (750 mM NaCl, 10 mM Tris-HCl, pH 7.0), and were resuspended in 100 μL of hybridization buffer. The PNA-beads were divided between two separate 1.5 mL centrifuge tubes. To one tube was added 1 nmol of 20-mer target DNA with sequence complementary to the PNA on the beads, and to the other (control) was added 1 nmol of noncomplementary 20-mer polyT DNA. The tubes were placed on a mechanical rotator and incubated overnight at room temperature. After incubation, the beads were washed with 0.4× SSC buffer 3 times. Previous studies of hybridized DNA-PNA 12-mers found melting temperatures of >62 °C and reductions of 15−20 °C for DNA with single base mismatch,[36] suggesting that the hybridized PNA-DNA used here is stable at the room temperature measurement conditions.

2.4. Zeta Potential, Electrophoretic Mobility, and Size Measurements. Following resuspension of the beads in 1 mM KCl, pH 7.0 at 25 °C, a Zetasizer Nano-ZS (Malvern Instruments) was used to characterize their zeta potential and electrophoretic mobility as well as their size using dynamic light scattering. The mean and mode diameters measured for the carboxylic acid beads were 3680 and 3580 nm, respectively, and the mean and mode diameters of the amine beads were 3250 and 3090 nm, respectively (Figure S1, Supporting Information).

2.5. Sensor Apparatus and Electrical Measurements. Two identical chambers made of polydimethylsiloxane (PDMS) connected by a 1 mm diameter opening were sealed to a glass microscope slide following activation with oxygen plasma. A prepulled borosilicate micropipet with outer diameter of 1 mm and nominal inner tip (pore) diameter of 2 μm was placed in the opening between the two chambers and sealed with vacuum grease so that the micropipet is the only connection between the two chambers (Figure 1). The platform was mounted on an inverted optical microscope (Leica DMIRB).

The chambers were filled with identical volumes of buffer (1 mM KCl, 10 mM HEPES, pH 7.0); Pt electrodes were placed in each chamber, away from the pipet entrances. A potential difference of 25 V was applied between the electrodes, and the resultant current was amplified by a transimpedance amplifier and logged using acquisition hardware at 1 kHz (PCI 6052E, National Instruments) and LabVIEW software (National Instruments). Data shown in the figures was processed in MATLAB with a fifth order Butterworth 100 Hz lowpass filter. After initial set up and baseline current recording, 10 μL of the bead suspension (in 1 mM buffered KCl) were injected into the micropipet and were observed optically while the system was monitored electrically. In the absence of applied voltage, motion of the beads within the capillaries was not observed.

3. RESULTS AND DISCUSSION

Initial experiments in this proof of concept demonstration relied on pH to modulate the charge of carboxylic acid- or amine-terminated polystyrene beads thereby manipulating their electrophoretic mobility and ability to effect pore blockage. At pH 7.0, the carboxylic acid beads carried substantial negative surface charge (zeta potential = −87 mV) due to the deprotonation of carboxylic acid groups ($pK_a \approx 4.5$) thereby making the beads responsive to an electric field. With the capillary tip at high electric potential (positively charged

dx.doi.org/10.1021/ja3059205 | J. Am. Chem. Soc. 2012, 134, 15880−15886

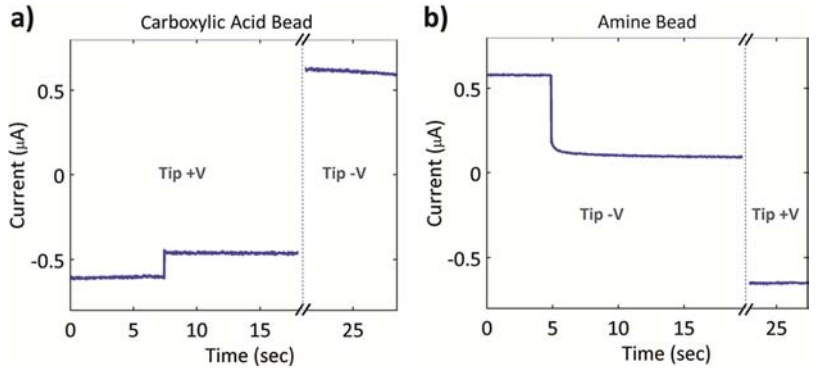

Figure 2. (a) Ionic current drop caused by pore blockade from a carboxylic acid-functionalized bead at pH 7.0. The blockade was reversible, as seen from the increase in current measured following reversal of the applied voltage (dashed line). (b) Ionic current drop caused by pore blockade from an amine-functionalized bead at pH 7.0. The blockade also was reversible, as seen from the increase in current measured following reversal of the applied voltage (dashed line).

electrode at tip), we observed the beads to move inside the capillary toward the pore ("sensing zone") and block it stably and indefinitely (Figure 2). Reversal of the applied potential caused the bead to move in the opposite direction, reopening the pore and returning the magnitude of the measured current to the initial value. This behavior was consistent and repeatably measurable, with some variation in the magnitudes of open capillary current and blocked current observed with different capillaries. (Table T1 in the Supporting Information summarizes repetition of carboxylic acid bead blockade measurement for four capillaries.) The bead blockade in one of the capillaries could not be reversed after the third blockade, but the other three capillaries were repeatably reversible and measured as long as desired. When the same experiments were conducted at pH 2.5 (below the carboxylic acid bead pK_a, measured zeta potential = −1.79 mV), the beads were observed to be immobile and no pore blockade could be achieved. Bead blockades were observed for applied potentials between 5 and 25 V; all measurements described below were conducted with an applied potential of 25 V.

Similar experiments were conducted with amine-terminated beads that are positively charged at pH 7.0 (pK_a ∼ 9.5, zeta potential = +69 mV at pH 7.0). When a potential of sign opposite to that used in the carboxylic acid bead experiments above was applied, the amine beads were observed to move toward the pore and block it, also producing stable, indefinite, and reversible reduction in the measured current (Figure 2) (data summarized in Table T2 in the Supporting Information). When repeated at pH 11.5, above the bead pK_a, the deprotonated and neutral amine beads (zeta potential = +6.3 mV) still moved in the same direction, but more slowly and with insufficient driving force to block the pore. This most likely resulted from electroosmotic flow caused by the deprotonated silanol (Si−OH) groups (pK_a ≈ 4) on the capillary surface. To confirm this, we microscopically examined the same beads and solution above the planar surface of a borosilicate glass Petri dish, and observed that the beads moved only when close to the glass surface, where the electroosmotic flow is largest. This is also consistent with the complete immobility of the carboxylic acid beads at acidic pH, since both the silanol groups on the capillary surface and the carboxylic acid groups on the beads are protonated and neutral. We presume that, in the experiments with the carboxylic acid beads at neutral pH, the force on the beads due to the electric field acting on the charged beads is greater than the opposing force due to electroosmotic flow, thereby enabling the beads to be driven to the pore.

Figure 2 shows a larger fraction of blocked current obtained with the amine beads compared to the carboxylic beads (81% vs 24%). In general, from measurements of the carboxylic acid beads in four capillaries and amine beads in three capillaries, the amine beads resulted in higher blockages (48−91%) than the carboxylic acid beads (4.7−66%) (Tables T1 and T2 and Figure S4 in Supporting Information), with some exception (Capillary 4 for carboxylic acid beads and Capillary 3 for amine beads). Optical observations indicated that the amine beads were typically immobilized closer to the capillary tip than the carboxylic acid beads, and it was common to observe some of the amine beads passing completely through the capillary tip. Since the amine beads were on average smaller than the carboxylic acid beads, this and additional observations suggest that the magnitude of the blockade is highly dependent on the relative sizes of the beads and the capillary tip.

In further support of this, a subsequent experiment with the carboxylic acid beads in a different capillary (with same nominal pore diameter of 2 μm) resulted in microscopic observation of some of the beads passing through the pore and, for those that blocked the pore, a larger reduction of current (63% average current blockage, Capillary 4, Table T1 in Supporting Information). Since the carboxylic acid beads in this experiment were drawn from the same batch as the carboxylic acid beads in previous experiments, complete passage of the beads through the pore suggests that the tip diameter of the micropipet was larger than the ones used in previous experiments. Additionally, measurement of the carboxylic acid beads in another capillary (Capillary 2 in Table T1 in Supporting Information) showed a reproducible bimodal blockade current (average blockade percentage of 24% and 6.9%) and two reproducible immobilization locations (with the 24% block occurring closer to the capillary tip (Figure S2, Supporting Information)) as the voltage was reversed and the experiment repeated. Since this measurement was obtained with one capillary, this suggests that beads of two different sizes or shapes were separately participating in the blockade.

The current measured for carboxylic acid beads passing completely through the tip of Capillary 4 (Figure S3, Supporting Information) displayed similar characteristics to previously reported measurements of beads traversing conical capillaries,[37,38] specifically with respect to the rapid decrease in blockade current as the bead passes through the tip to the

external solution. However, we do see a difference from this previous work in that the passage time of the bead through the tip is approximately 40 ms, significantly longer than the 1 ms times previously reported for 2 μm diameter colloids. This is most likely due to the transport of the carboxylic acid beads being slowed by the opposing electroosmotic flow. This is also supported by experiments with the amine beads, which were observed microscopically to pass through the capillary tip but no blockade currents were able to be resolved with 1 kHz data acquisition. The magnitude of the reduction in current measured during the passage of the carboxylic acid beads (12%, an increase in resistance of 5.65 MΩ) was consistent with previous work reported with similar systems.[38,39] We also developed a simple analytic model calculating the increase in resistance caused by the presence of a spherical particle in a conical channel with circular cross-section based on Gregg and Steidley's model of resistive pulse from particles in a cylindrical channel,[40,41] described in the Supporting Information.

The model predicts increasing blockade resistance with increasing ratio of particle radius to capillary radius r_p/r_c. For a spherical particle fully contacting the interior of a conical capillary with circular cross-section, r_p/r_c is close to unity and the model predicts complete block of the current. None of our measurements showed complete blockades, although one capillary measured with the amine beads showed 90% average block (Capillary 2, Table T2, Supporting Information). These measurements of incomplete block indicate that the particles did not fully contact the capillary interior, possibly due to noncircular cross sections of the particle or capillary, presence of asperities on the bead or capillary surfaces, or adherence of the particle to the capillary wall before full contact. Evidence from the previously discussed carboxylic acid beads with Capillary 2 supports variation in bead size or shape in that the bimodal distribution of blocked currents was quite repeatable and correlated with microscopic observations.

Although the model assumes circular cross-section of the particle and conical capillary, its parametrization in r_p/r_c can be seen alternatively in terms of the particle and capillary cross sections as $(r_p/r_c) = (\text{Area}_{\text{particle}})^{1/2}/(\text{Area}_{\text{capillary}})^{1/2}$ or $r_p/r_c = (1 - \text{Area}_{\text{gap}}/\text{Area}_{\text{capillary}})^{1/2}$ and therefore as r_p/r_c increases, $\text{Area}_{\text{gap}}/\text{Area}_{\text{capillary}}$ decreases. In this way, we may understand that elliptical cross sections of either the particles or the capillary would create larger blockades for smaller particles (thus also blocking closer to the capillary tip) because the cross-sectional area of the gap would decrease, roughly translating to an increased r_p/r_c in our model. Therefore in our model, the size of the resistance increase depends on eccentricity of the particle or capillary cross sections and the particle size. For beads plugging pores, we experimentally observed resistance increases in the range of 38−430 MΩ for amine beads (48−91% block) and 2−78 MΩ for carboxylic acid beads (4.7−66% block) (Tables T1 and T2, Supporting Information). For the smaller 3150 nm diameter amine beads, the model yields resistance increases of 38−430 MΩ for r_p/r_c of 0.87−0.985. For 3600 nm diameter carboxylic acid beads, the model yields ΔR of 2−78 MΩ for r_p/r_c of 0.54−0.93.

We modeled the bead electrophoretic force by equating it to the drag force on the bead when it is moving with constant speed. The measured mobility is the proportionality constant between the speed and the electric field. By modeling the capillary as a simple cone, we estimated the electric field in the capillary as a function of position and found forces between 1.36 and 5.44 nN as the capillary radius tapered from two bead radii to one bead radius (Supporting Information).

Next, nucleic acid detection was measured using 20-mer polyA ssDNA as a simple target sequence and PNA-beads conjugated with 12-mer polyT PNA as the complementary probe. To assess the PNA conjugation to the carboxylic acid beads, the beads' zeta potential before PNA conjugation was measured to be −87 mV, after ethanolamine capping +5.75 mV, and after three washes with 0.4× SSC buffer −4.39 mV. After capping and washing, the beads were observed to aggregate. Without incubation with DNA, the PNA-beads in the micropipet were seen to follow the electroosmotic flow away from the pipet tip, indicating that the PNA-beads alone were unable to block the pore. Incubation of the PNA-beads with polyA target ssDNA resulted in well-dispersed beads with a measured zeta potential of −71.1 mV, and motion toward the pipet tip in the same applied voltage, ultimately blocking it (Figure 3b). These current blockades were stable, indefinite, and reversible.

In a control experiment, the same polyT PNA-beads as above were incubated with noncomplementary 20-mer polyT ssDNA, resulting in a bead preparation with a measured zeta potential of −46.7 mV, which indicated a significant amount of nonspecific binding of DNA to the beads. Microscopic observation of the control beads showed movement of the beads to the pore, which they temporarily blocked and then moved back down the pipet away from the pore along with the electroosmotic flow. Simultaneous electrical measurement showed a transient current blockade of up to approximately 10 s long (Figure 3d). This transient blockade was observed infrequently, with most of the control beads unable to block the pore.

The control and target experiments were repeated at least three times; measured zeta potentials and electrophoretic mobilities are listed in Table 1 with the qualitative results of the electrical measurements (Data summarized in Tables T3 and T4 in the Supporting Information). Quantitatively, the magnitude of the blockades measured for the target DNA was consistent between the three capillaries (average blockades: 22.0%, 25.6%, and 25.6%; Table T3 in the Supporting Information). The blockade of one of the capillaries could not be reversed after five measurements.

We hypothesize that incubation of the beads with ssDNA results in a significant amount of nonspecific binding for both complementary and noncomplementary sequences. In the control experiments, the DNA binding to the bead is entirely nonspecific and presumably less strongly bound than the complementary DNA. Still, the beads with nonspecifically bound DNA are negatively charged and electrophoretically mobile, allowing them to be driven to the pore. In the pore, the electric field is sufficiently strong to remove the nonspecifically bound DNA from the bead, which causes a reduction in bead charge and electrophoretic mobility, enabling the electroosmotic flow to exceed the electrophoretic force and carry the bead away from the pore. For complementary DNA sequences, the bead likely carries specific and nonspecifically bound DNA but the strong electric field is insufficient to remove the hybridized DNA from the bead (Figure 3a and c).

To estimate these forces, we used the model described above to analyze the electric field near a trapped bead and to determine the electric force on a 20-mer ssDNA on the bead surface (Supporting Information). On the basis of the average currents measured for PolyA ssDNA-PolyT PNA beads in three

dx.doi.org/10.1021/ja3059205 | J. Am. Chem. Soc. 2012, 134, 15880−15886

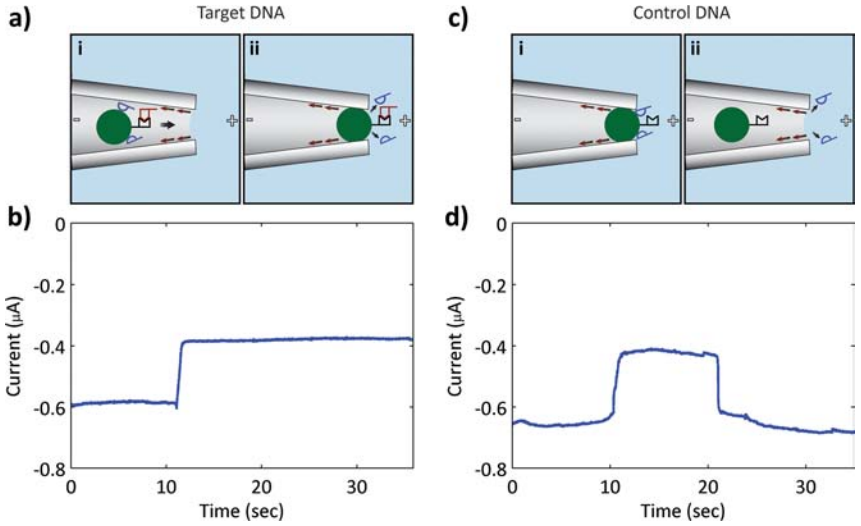

Figure 3. Schematic of motion of PNA-bead under an applied potential and resultant measured current. (a) (i) PNA-beads (green) with nonspecifically bound ssDNA and specifically bound ssDNA hybridized to PNA on the bead are negatively charged and electrophoretically mobile. (ii) In the strong electric field at the pore tip, the nonspecifically bound DNA is removed from the bead, but the hybridized DNA is not, leaving the bead with sufficient negative charge to remain blocking the pore indefinitely. (b) Measured permanent current blockade for PNA-beads incubated with complementary polyA DNA, corresponding to (a). (c) For PNA-beads incubated with only noncomplementary DNA, any DNA bound to the bead is nonspecific; the strong electric field at the pore tip removes the nonspecifically bound DNA, reducing the bead's charge sufficiently so that the electroosmotic flow (red arrows) is able to remove the bead from the pore tip (ii). (d) Transient current blockade measured for PNA-beads incubated with noncomplementary polyT DNA, corresponding to (c).

Table 1. Summary of Experimental Results for Target and Control Samples[a]

target PolyA			control PolyT		
zeta potential (mV)	mobility (10^{-8} $m^2/(V\ s)$)	results	zeta potential (mV)	mobility (10^{-8} $m^2/(V\ s)$)	results
−71.1 ± 4.0	−5.57	Permanent block	−46.7 ± 4.28	−3.66	Transient block
−59.3 ± 5.1	−4.65	Permanent block	−36.8 ± 4.47	−2.88	No block
−59.8 ± 4.7	−4.69	Permanent block	−32.1 ± 5.3	−2.52	No block

[a]Zeta potential and electrophoretic mobility measured after ssDNA incubation and results of micropipet electrical measurements.

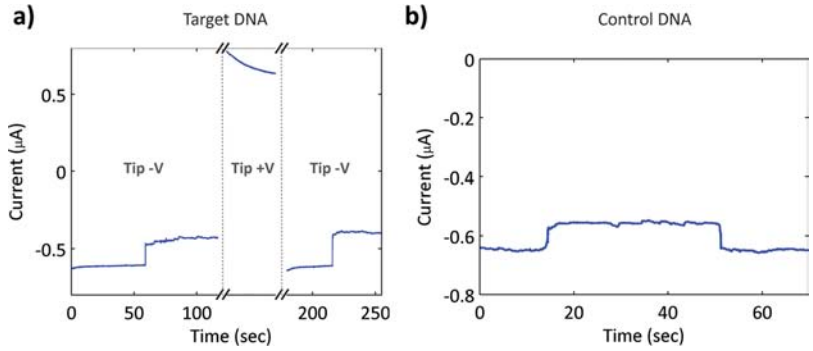

Figure 4. (a) Permanent ionic current drop caused by beads incubated with target anthrax ssDNA. The blockade was reversible and repeatable, as seen by reversals of the applied voltage (dashed lines). (b) Transient ionic current drops were seen occasionally with beads incubated with the noncomplementary, control ssDNA.

capillaries (Table T3, Supporting Information), a force of 13.9 pN is obtained from the model for the 20-mer ssDNA on the bead surface. This force is less than the 57 pN rupture forces measured for 8 bp DNA-PNA with optical tweezers.[42]

To further investigate the selectivity of the sensor, we detected ssDNA with a nonrepeating sequence, a 12-mer portion of a gene encoding the anthrax lethal factor.[43] To allow direct comparison with the previous experiment detecting 20-mer ssDNA, we added an 8-mer polyA tail to the 12-mer anthrax sequence. To enhance the binding of complementary ssDNA and minimize nonspecific binding, a PEG spacer was added to the amine-functionalized 12-mer complementary PNA capture probe.[44] After PNA conjugation, capping with ethanolamine, and washing, the measured zeta potential of this PNA-bead preparation was −2.75 mV. The PNA-beads were divided into two volumes, one incubated with 20-mer target anthrax ssDNA and the other with control 20-mer polyT ssDNA. Measured zeta potentials after incubation were −56.7 mV for target beads and −39.0 mV for control beads. As with the previous experiments described above, the presence of complementary DNA led to permanent blockades, whereas its absence led to transient or no blockade (Figure 4) (Videos,

dx.doi.org/10.1021/ja3059205 | J. Am. Chem. Soc. 2012, 134, 15880−15886

Table 2. Summary of Experimental Results for Target and Control Samples[a]

target anthrax			control PolyT		
zeta potential (mV)	mobility (10^{-8} $m^2/(V\ s)$)	results	zeta potential (mV)	mobility (10^{-8} $m^2/(V\ s)$)	results
−56.7 ± 6.4	−4.44	Permanent block	−39.0 ± 6.50	−3.06	Transient block
−53.5 ± 5.1	−4.19	Permanent block	−30.6 ± 5.78	−2.40	No block
−50.6 ± 3.7	−3.96	Permanent block	−32.8 ± 4.50	−2.57	No block

[a]Zeta potential and electrophoretic mobility measurements after each hybridization experiment and results of electrical measurements.

Table 3. Summary of Experimental Results for Target and Single Base Mismatch Control Samples[a]

target anthrax			anthrax LF single base mismatch		
zeta potential (mV)	mobility (10^{-8} $m^2/(V\ s)$)	results	zeta potential (mV)	mobility (10^{-8} $m^2/(V\ s)$)	results
−51.1 ± 5.6	−4.01	Permanent block	−45.3 ± 4.38	−3.55	Transient block
−50.3 ± 4.2	−3.95	Permanent block	−44.8 ± 3.72	−3.52	Transient block
−50.9 ± 3.9	−3.99	Permanent block	−41.4 ± 5.23	−3.24	Transient block

[a]Zeta potential and electrophoretic mobility measurements after each hybridization experiment and results of electrical measurements.

Table T5 (Capillaries 1−3), and Table T6 in Supporting Information). Even in experiments with the control DNA in which transient blockades were measured, only a few beads were seen to transiently block the current, with the majority of the beads being inadequately mobile in the electric field to block the pore. These experiments were repeated three times and the results are summarized in Table 2.

The capillary blockade and its magnitude was highly repeatable. In six capillaries tried (three listed in Table 2 and three discussed below and listed in Table 3), blockades were observed for all six (average blockade: 21.5%, 23.0%, 24.6%, 21.8%, 23.9%, and 21.1%; Table T5, Supporting Information). In each of the capillaries measured, following blockade, the voltage was reversed to remove the bead from the capillary tip to attempt further blockades. In one of the six capillaries, after five detection events, the bead was not able to be removed from the blockade site with reversal of applied voltage and the experiment was terminated.

To investigate the sequence specificity of the sensor, we created a 20-mer ssDNA with the same sequence as the 20-mer ssDNA for the anthrax LF experiment described above but with a single base mismatch. The measured zeta potential after PNA conjugation, capping with ethanolamine, and washing was −7.39 mV. As described above, the PNA-beads were divided into two volumes, one incubated with the anthrax LF ssDNA and one with the single base mismatch ssDNA (Table T5 (Capillaries 4−6) and Table T7, Supporting Information). Table 3 summarizes the results of three separate experiments, which are consistent with our previous results described above. Occasional transient blockades were observed in the presence of the mismatch DNA sample; permanent blockades were recorded only in the presence of target anthrax ssDNA.

Since the melting temperature for the single base mismatched DNA is above room temperature, the mismatched DNA-PNA is stably hybridized following incubation of the DNA with the PNA-beads. The measurement of the transient block could result from the mismatched hybrid having a sufficiently low force of dissociation that the DNA strands are removed in the strong electric field of the pore, or the number of mismatched strands hybridized to the bead could be less and the electric field of the pore is removing nonspecifically bound DNA from the bead as described above in Table 2 and Figure 4. With either or both of these mechanisms contributing, there was no permanent blockade resulting from the single base mismatched DNA.

Comparison of beads incubated with complementary target ssDNA in Table 1 (target: poly A) and Tables 2 and 3 (target: Anthrax-LF) shows that the magnitudes of the zeta potentials and mobilities in Table 1 were larger than those in Tables 2 and 3. A possible explanation for these results is the lack of registration required for the hybridization of polyA ssDNA, compared to the exact registration required for hybridization of Anthrax ssDNA. Longer ssDNA targets may improve the electrophoretic mobility of the hybridized beads, while longer strands of nonspecifically bound ssDNA would still be expected to detach from the bead in the strong electric field at the sensing zone to result in only transient ionic current blockades.

The limits of detection were probed by serially diluting the 20-mer target anthrax ssDNA in hybridization buffer and repeating the incubation with PNA beads and nanopore measurement as described above (Table T8, Supporting Information). Pore blockade was observed down to a concentration of 10 pM. At this concentration, we observed some beads only transiently blocking the pore before permanent block was achieved, indicating the presence of both nonspecific and complementary ssDNA bound to the beads, as well as a smaller amount of bound complementary DNA. We are currently working to reduce the concentration limit of detection of our micropipet-based system through the use of longer target ssDNA oligomers.

Overall, our system performed as expected for detection of specific DNA sequences. Using the conditions described, polyA or anthrax DNA were successfully detected in every capillary tried (nine capillaries total), with no false positives (no permanent blockade) observed in any capillary (nine capillaries total), including ssDNA with only a single base mismatch. The lowest DNA concentration successfully detected with our unoptimized system was ∼10 pM, an unimpressive detection level compared to other published approaches, including a PNA sandwich-hybridization assay for anthrax with a DNA detection limit of as low as 10 zmol.[31] Yet, this binary detection system could exhibit a very low detection limit if the system were scaled down such that a submicrometer PNA-bead conjugate would assume sufficient charge for electrophoretic mobility and pore blocking upon binding one or a few target DNA molecules. Of course this low detection limit comes at the expense of the capability to determine target DNA concen-

tration. Nevertheless, as discussed in the Introduction, there are a number of important applications where a binary (yes/no) signal for the presence/absence of the DNA target is sufficient. Further, the large and sustained reduction in current resulting from the blockade of the pore by a PNA-bead conjugate with bound target DNA provides an easily detectable signal for the presence of the DNA target that can be displayed with simple electronics. Using a simple inverting operational amplifier and light emitting diodes, we constructed a binary indicator of the target DNA detection, demonstrating its potential application in a simple, potentially low-cost device. In the future, we will work to scale down using silicon micromachining technology and to optimize this system in order to achieve meaningful detection limits and to apply it to the sensing of NA in biological samples.

■ ASSOCIATED CONTENT

Supporting Information

Supporting Information contains the following: DLS diameter measurements of carboxylic acid and amine beads; a list of unblocked and blocked currents measured for all capillaries; microscopic images of beads immobilized at a capillary tip; measurements of current during passage of two carboxylic acid beads completely through a capillary tip; measurements of zeta potential and occurrence of blockade as a function of Anthrax LF DNA concentration; description of a model calculating change in resistance from a spherical particle in a conical channel and use of this model to estimate forces on beads within the capillary and on DNA on the surface of immobilized beads; and videos of complementary Anthrax DNA PNA-bead immobilization in a capillary and the transient immobilization of noncomplementary polyT DNA (Anthrax PNA)-bead in a capillary. This material is available free of charge via the Internet at http://pubs.acs.org.

■ AUTHOR INFORMATION

Corresponding Author

*harold@seas.ucla.edu; schmidt@seas.ucla.edu

Notes

The authors declare no competing financial interest.

■ ACKNOWLEDGMENTS

This publication was supported by grant number R21HG006157-01 from the National Human Genome Research Institute (NHGRI) at the National Institutes of Health. The authors thank members of Schmidt laboratory at UC Los Angeles especially Peter Du and Ahmad El-Arabi for their valuable help. We also thank Prof. Tatiana Segura and her research group for assistance with the Zetasizer measurements.

■ REFERENCES

(1) Chee, M.; Yang, R.; Hubbell, E.; Berno, A.; Huang, X. C.; Stern, D.; Winkler, J.; Lockhart, D. J.; Morris, M. S.; Fodor, S. P. A. *Science* **1996**, *274*, 610.
(2) Maitra, A.; Cohen, Y.; Gillespie, S. E. D.; Mambo, E.; Fukushima, N.; Hoque, M. O.; Shah, N.; Goggins, M.; Califano, J.; Sidransky, D.; Chakravarti, A. *Genome Res.* **2004**, *14*, 812.
(3) Pellestor, F.; Paulasova, P.; Hamamah, S. *Curr. Pharm. Des.* **2008**, *14*, 2439.
(4) Chen, S.-H.; Wu, V. C. H.; Chuang, Y.-C.; Lin, C.-S. *J. Microbiol. Methods* **2008**, *73*, 7.
(5) Lam, B.; Fang, Z.; Sargent, E. H.; Kelley, S. O. *Anal. Chem.* **2012**, *84*, 21.
(6) Lubin, A. A.; Lai, R. Y.; Baker, B. R.; Heeger, A. J.; Plaxco, K. W. *Anal. Chem.* **2006**, *78*, 5671.
(7) Reynolds, R.; Walker, K.; Varlaro, J.; Allen, M.; Clark, E.; Alavaren, M.; Erlich, H. *J. Forensic Sci.* **2000**, *45*, 1210.
(8) Wu, Y. Y.; Csako, G. *Clin. Chim. Acta* **2006**, *363*, 165.
(9) Teles, F. R. R.; Fonseca, L. P. *Talanta* **2008**, *77*, 606.
(10) Campbell, C. T.; Kim, G. *Biomaterials* **2007**, *28*, 2380.
(11) Hassibi, A.; Vikalo, H.; Riechmann, J. L.; Hassibi, B. *Nucleic Acids Res.* **2009**, *37*, e132.
(12) Howorka, S.; Cheley, S.; Bayley, H. *Nat. Biotechnol.* **2001**, *19*, 636.
(13) Singer, A.; Wanunu, M.; Morrison, W.; Kuhn, H.; Frank-Kamenetskii, M.; Meller, A. *Nano Lett.* **2010**, *10*, 738.
(14) Wang, Y.; Zheng, D.; Tan, Q.; Wang, M. X.; Gu, L.-Q. *Nat. Nanotechnol.* **2011**, *6*, 668.
(15) Balagurusamy, V. S. K.; Weinger, P.; Ling, X. S. *Nanotechnology* **2010**, *21*, 335102.
(16) Nielsen, P.; Egholm, M.; Berg, R.; Buchardt, O. *Science* **1991**, *254*, 1497.
(17) Li, K.; Liu, B. *Anal. Chem.* **2009**, *81*, 4099.
(18) Ross, P. L.; Lee, K.; Belgrader, P. *Anal. Chem.* **1997**, *69*, 4197.
(19) Wang, J.; Nielsen, P. E.; Jiang, M.; Cai, X.; Fernandes, J. R.; Grant, D. H.; Ozsoz, M.; Beglieter, A.; Mowat, M. *Anal. Chem.* **1997**, *69*, 5200.
(20) Komiyama, M.; Ye, S.; Liang; Yamamoto, Y.; Tomita, T.; Zhou, J.-M.; Aburatani, H. *J. Am. Chem. Soc.* **2003**, *125*, 3758.
(21) Wang, C.; Zhan, R.; Pu, K.-Y.; Liu, B. *Adv. Funct. Mater.* **2010**, *20*, 2597.
(22) Singh, R. P.; Oh, B.-K.; Choi, J.-W. *Bioelectrochemistry* **2010**, *79*, 153.
(23) Brandt, O.; Hoheisel, J. D. *Trends Biotechnol.* **2004**, *22*, 617.
(24) Wang, J.; Palecek, E.; Nielsen, P. E.; Rivas, G.; Cai, X.; Shiraishi, H.; Dontha, N.; Luo, D.; Farias, P. A. M. *J. Am. Chem. Soc.* **1996**, *118*, 7667.
(25) Brandt, O.; Feldner, J.; Stephan, A.; Schröder, M.; Schnölzer, M.; Arlinghaus, H. F.; Hoheisel, J. D.; Jacob, A. *Nucleic Acids Res.* **2003**, *31*, e119.
(26) Gaylord, B. S.; Heeger, A. J.; Bazan, G. C. *Proc. Natl. Acad. Sci.* **2002**, *99*, 10954.
(27) Raoof, J. B.; Ojani, R.; Golabi, S. M.; Hamidi-Asl, E.; Hejazi, M. S. *Sens. Actuators, B* **2011**, *157*, 195.
(28) Kerman, K.; Matsubara, Y.; Morita, Y.; Takamura, Y.; Tamiya, E. *Sci. Technol. Adv. Mater.* **2004**, *5*, 351.
(29) Jágerszki, G.; Gyurcsányi, R. E.; Höfler, L.; Pretsch, E. *Nano Lett.* **2007**, *7*, 1609.
(30) Ali, M.; Neumann, R.; Ensinger, W. *ACS Nano* **2010**, *4*, 7267.
(31) Zhang, N.; Appella, D. H. *J. Am. Chem. Soc.* **2007**, *129*, 8424.
(32) Karhanek, M.; Kemp, J. T.; Pourmand, N.; Davis, R. W.; Webb, C. D. *Nano Lett.* **2005**, *5*, 403.
(33) Steinbock, L. J.; Otto, O.; Chimerel, C.; Gornall, J.; Keyser, U. F. *Nano Lett.* **2010**, *10*, 2493.
(34) Fu, Y.; Tokuhisa, H.; Baker, L. A. *Chem. Commun.* **2009**, 4877.
(35) Umehara, S.; Karhanek, M.; Davis, R. W.; Pourmand, N. *Proc. Natl. Acad. Sci.* **2009**, *106*, 4611.
(36) Ratilainen, T.; Holmén, A.; Tuite, E.; Nielsen, P. E.; Nordén, B. *Biochemistry* **2000**, *39*, 7781.
(37) Lan, W.-J.; Holden, D. A.; Zhang, B.; White, H. S. *Anal. Chem.* **2011**, *83*, 3840.
(38) Steinbock, L. J.; Stober, G.; Keyser, U. F. *Biosens. Bioelectron.* **2009**, *24*, 2423.
(39) Stober, G.; Steinbock, L. J.; Keyser, U. F. *J. Appl. Phys.* **2009**, *105*, 084702.
(40) Gregg, E. C.; Steidley, K. D. *Biophys. J.* **1965**, *5*, 393.
(41) DeBlois, R. W.; Bean, C. P. *Rev. Sci. Instrum.* **1970**, *41*, 909.
(42) Zohar, H.; Hetherington, C. L.; Bustamante, C.; Muller, S. J. *Nano Lett.* **2010**, *10*, 4697.
(43) Park, S.-J.; Taton, T. A.; Mirkin, C. A. *Science* **2002**, *295*, 1503.
(44) Hurst, S. J.; Lytton-Jean, A. K. R.; Mirkin, C. A. *Anal. Chem.* **2006**, *78*, 8313.